Pergamon

SCIENCE DIRECT®

Bioorganic & Medicinal Chemistry 11 (2003) 2355–2365

BIOORGANIC & MEDICINAL CHEMISTRY

Synthesis and Evaluation of Peptidomimetics That Bind DNA

Jeffrey A. Turk and David B. Smithrud*

Department of Chemistry, University of Cincinnati, Cincinnati, OH 45221-0172, USA

Received 22 March 2002; accepted 7 November 2002

Abstract—A peptidomimetic template, consisting of a hydrophobic scaffold, a dansyl fluorophore, and an Arg-His recognition strand, was tested as a simple mimic of zinc finger 2 of the Zif268 protein. Association constants (K_A's) were on the order of 10^5 M^{-1} for complexes formed between the mimetic and duplexes $d(CGGGAATTCCCG)_2$ and $d(AAAAAAAAATTTTTTTT)_2$. Modest selectivity was observed for the GC-rich DNA in a 0.5 M NaCl/buffer (0.1 M phosphate, pH 7.0) solution. Differences in K_A's along with observed CD profiles suggest that the mimetic associated with the duplexes using different binding modes. The DNA duplexes had weaker interactions with the free Arg-His recognition strand, the dansyl functional group, and a scaffold that contained only glycines as the recognition strand. The scaffold most likely provides for greater van der Waal's interactions, a larger hydrophobic effect upon association, and reduces the freedom of motion of the side chains. This last effect was confirmed by molecular mechanics calculations and by the fact that the mimetic suffered a smaller loss of entropic energy upon association than the free recognition strand. These studies show that the synthetic scaffold is a promising platform in which peptides can be attached to increase their affinity and possibly selectivity for DNA targets.

Introduction

The zinc finger is one of the most ubiquitous and abundant DNA-binding motifs found in eukaryotes, and proteins that display zinc-fingers specifically bind a diverse set of DNA sequences involved with gene regulation.[1] For the Cys_2-His_2 class of zinc fingers, each finger contains approximately 30 amino acids held in a ββα-motif, which is stabilized by a zinc ion. A relatively simple binding mechanism has been proposed for the interaction between a zinc finger and its DNA-target. Early studies suggested a 1:1 amino acid to base code existed that could be used to predicate and control the finger's specificity and affinity for DNA.[2] A recognition code was postulated because residues in the α-helix at a specific position interact with a base at a specific site, and these interactions are well conserved among a variety of zinc fingers. Recent studies of modified zinc fingers—created randomly through phage display technology—suggest that a code does not exist or that it is more complicated than originally thought.[3]

Deciphering of the zinc finger code could lead to designer DNA-binding proteins or compounds that could be used for gene therapy and controlling gene regulation.[4,5] Promising results have been obtained for modified zinc finger proteins that bind the TATA box, a p53 binding site, and a nuclear receptor element with nanomolar association constants, which discriminate against nonspecific DNA.[6] A family of zinc finger domains that recognize all combinations of 5′-GNN-3′ sequence has been constructed through phage display library technology.[3] Inorganic complexes of Zn^{2+} and short peptides have also shown affinity for DNA.[7–12]

Our research goals are to create compounds that selectively bind DNA and obtain insights into the code used by zinc finger domains to recognize DNA. The zinc fingers of the Zif268 protein were chosen as the initial model system because they appear to use only a few amino acids to specifically recognize DNA. Arginine and histidine residues of zinc finger 2, which are held on a single face of an α-helix, form H-bonds with consecutive guanine residues, whereas two arginine residues of finger 1 or 3 recognize alternating guanine residues.[13] The question we addressed in this study is whether the simplest code of placing Arg and His residues on a peptidomimetic scaffold, as a mimic of zinc finger 2 of Zif268, provides enough structure to obtain affinity or selectivity in DNA association. The mimic contains three domains: a hydrophobic core, a recognition stand (an Arg-His dipeptide), and a dansyl fluorophore. Each domain

*Corresponding author. Tel.: +1-513-556-9254; fax: +1-513-556-9239; e-mail: david.smithrud@uc.edu

0968-0896/03/$ - see front matter © 2003 Elsevier Science Ltd. All rights reserved.
doi:10.1016/S0968-0896(02)00646-6

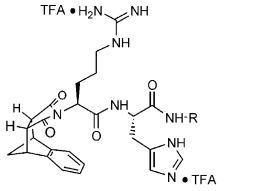

1 a R = NHMe
b R = DAE·TFA

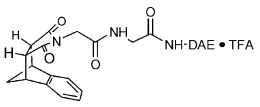

2

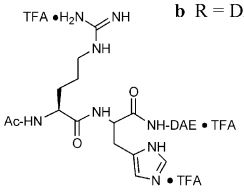

3

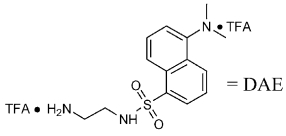

4

could potentially interact with DNA. To assess whether one or more domains are important for recognition, each piece of the mimetic was synthesized and its ability to bind DNA was determined. Because zinc finger 2 selectively binds consecutive G-residues, and finger 1 or 3 bind alternating G-residues, the modified Dickerson dodecamer[14] d(CGGGAATTCCCG)$_2$ (hereafter referred to as mDd) was chosen as a target for the mimetic. The d(AAAAAAAAATTTTTTTTT)$_2$ (referred to as d(A9T9)$_2$) duplex was also chosen to determine if the mimetic preferentially binds GC-rich DNA.

Results

Design and synthesis of the templates

Peptidomimetic template **1a** contains a polycyclic imide scaffold that supports the recognition strand, which contains key residues used by zinc finger 2 of Zif268 to bind DNA. A dansyl (DAE) fluorophore was added to mimetic **1a**, giving mimetic **1b**, to investigate DNA association through fluorescence assays. Compounds **2–4** were constructed and tested to determine how important the scaffold, recognition strand, and dansyl groups, respectively, are for complex formation. Compounds that contain the aromatic scaffold were created starting from endo-*N*-methyl-2,3-dicarboxyimido-5,6-benzobicyclo[2.2.1]heptane **5**; the Diels–Alder adduct of maleic anhydride and isoindene (Scheme 1).[15] The 2-mesitylenesulfonyl (MTS) protected arginine imide **6** was created by opening anhydride **5** with Arg(MTS) and then closing to the imide upon the addition of CDI in the presence of DIEA. Histidine methyl ester dihydrochloride was added to imide **6** in the presence of DCC/HOBT to give the terminal methyl ester. Amidation using excess *N*-methyl amide followed by deprotection of MTS from the arginine side chain using TFA/TFMSA thioanisole (8:1:1) gave peptidomimetic mimetic **1a**.

The other compounds were constructed in a similar manner except that a dansyl group was also attached. Commercially available Boc-His(Boc) **7** was activated using traditional DCC/HOBT methods, coupled to *N*-(2-aminoethyl)-5-(dimethylamino)-naphthalene sulfonamide (DANSA),[16] and deprotected with 30% TFA in methylene chloride to give His-DAE **8**. Mimetic **1b** was created by coupling Arg(MTS) imide **6** to His-DAE **8** followed by deprotection of the MTS protecting group as previously described. Opening of anhydride **5** with glycine-glycine methyl ester[17] in the presence of DIEA followed by the addition of CDI resulted in formation of the *N*-Gly-Gly methyl ester imide **9**, which was hydrolyzed under mild basic conditions to give acid **10**. This acid was coupled to His-DAE **8** using DCC/HOBT methods to yield compound **2**. Synthesis of the recognition strand **3** began with the coupling of commercially available Boc-Arg(Boc)$_2$ **11** with His-DAE **8** to give Boc-Arg(Boc)$_2$-His-DAE **12**. The arginine residue was deprotected using a 30% TFA in methylene chloride solution. Treatment of the trifluoroacetate salt with lithium hydroxide, followed by a single equivalent of acetic anhydride, gave the recognition strand **3**.

Fluorescence spectra. The fluorescence of compounds **1b–4** was quenched with the addition of mDd or d(A9T9)$_2$ (Fig. 1). A greater amount of quenching occurred for mimetic **1b** with either mDd or d(A9T9)$_2$ when compared to compounds **2–4**. There were no significant changes in the shapes of the curves or the existence of isosbestic points. Changes in the fluorescence spectra were used to derive association constants (Table 1). The fluorescence intensity observed at 570 nm was plotted against the concentration of DNA (Fig. 2), and K_A's were derived using a modified Stern–Volmer equation.[18] The intrinsic fluorescence of DNA at this wavelength (less than 20% of the dansyl fluorescence of mimetic **1b**) was subtracted prior to K_A determination. The linearity of the plots suggests that a single association constant accurately represents the strength of a complex formed between one of the compounds and DNA at the concentrations used in the assays.

Mimetic **1b**, which has a hydrophobic core, recognition strand, and dansyl group, has a higher affinity for mDd as compared to compounds **2–4**. Removing the positively charged side chains and the methylenes of the Arg-His recognition strand gives an approximate 5-fold drop in affinity (mimetic **1b** vs compound **2**). A 4-fold drop in affinity for mDd is observed for the recognition strand without the hydrophobic scaffold (mimetic **1b** vs compound **3**). DANSA **4** also associates weakly with the DNA.

To test the binding specificity of the peptidomimetic templates for GC regions, we determined the association constants for their complexes with d(A9T9)$_2$. The fairest test would have been to compare mDd with d(A6T6)$_2$ that is also a dodecamer duplex. Unfortunately, the calculated melting temperature for duplex d(A6T6)$_2$ is 24 °C, which means at the experimental temperature of 25 °C, the DNA exists as an approximate equal mixture of monomers and dimers. Therefore, 18-mer d(A9T9)$_2$, which has a melting temperature of 39 ± 1 °C, was chosen as one model duplex to ascertain binding selectivity. Association between d(A6T6)$_2$ and mimetic **1b** was also investigated. K_A for this complex was obtained by assuming that 50% of the DNA existed in the duplex form. The value for $K_{A\text{-}12mer}$ matched $K_{A\text{-}18mer}$ once this latter value was reduced by 33%

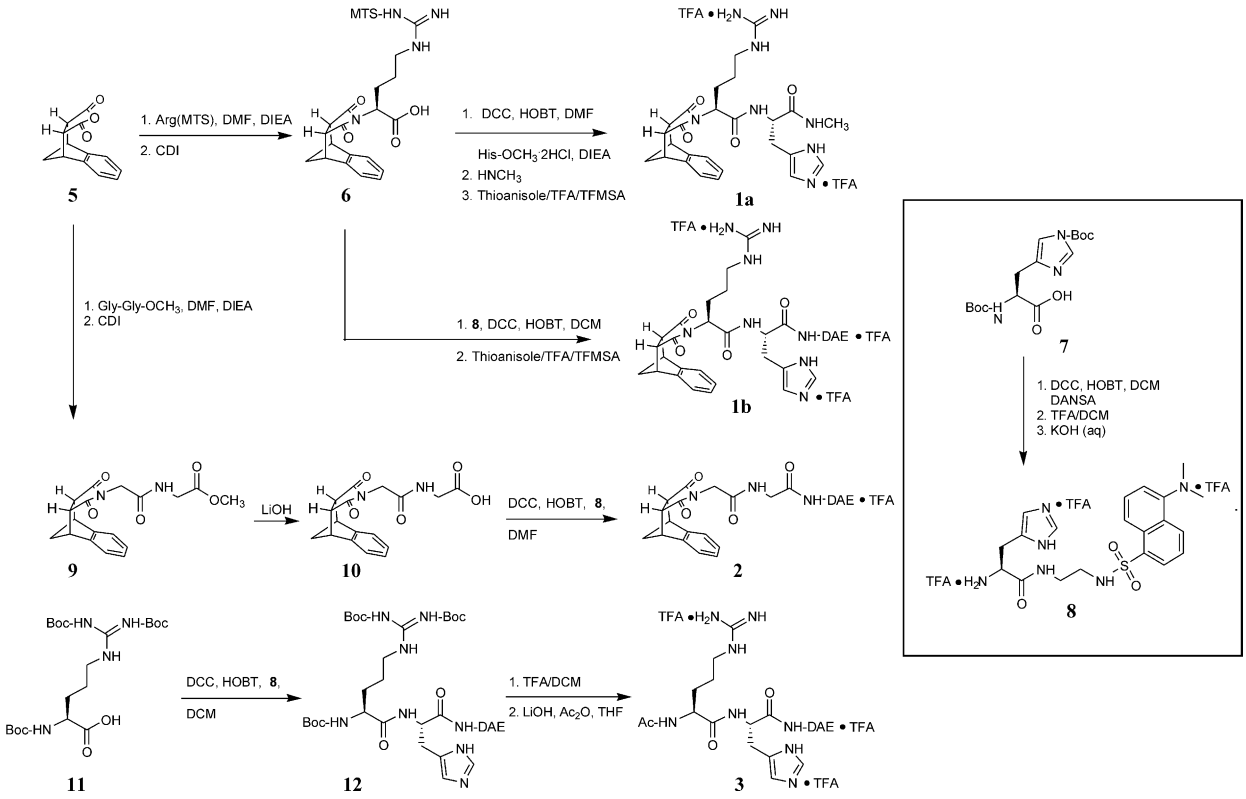

Scheme 1.

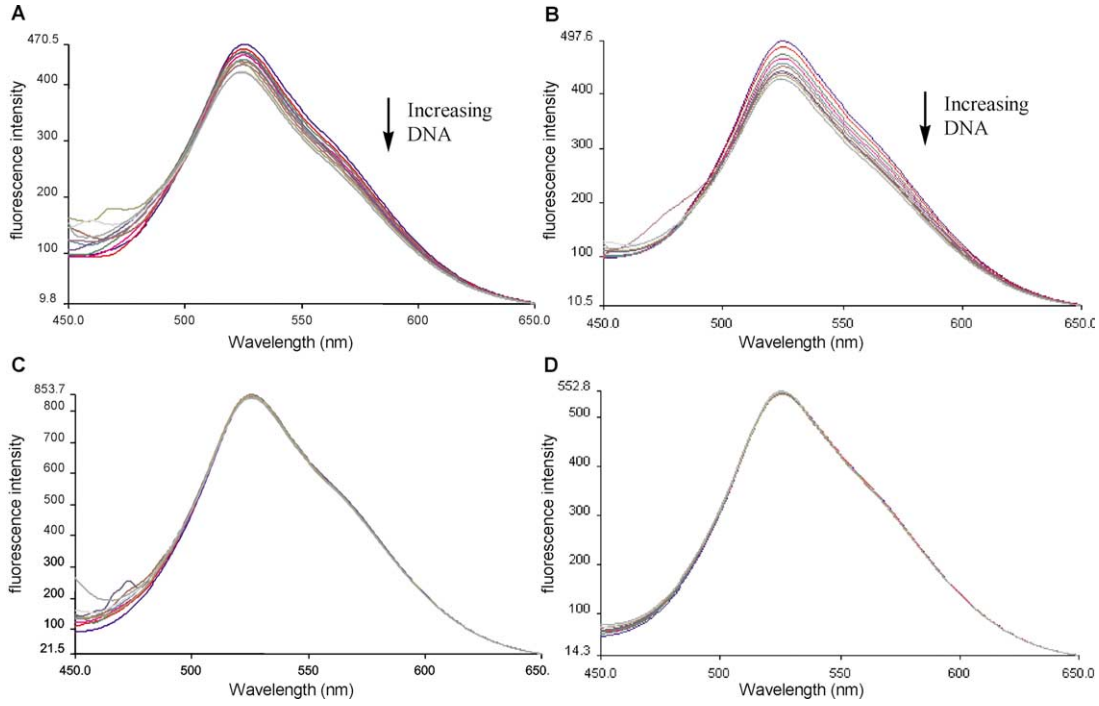

Figure 1. Representative fluorescence quenching assays of mimetic **1b** binding to (A) mDd and (B) d(A9T9)$_2$ and compound **3** binding to (C) mDd and (D) d(A9T9)$_2$ in 0.1 M phosphate buffer pH 7.0 at 25 °C. Mimetic **1b** and compound **3** were held at a constant concentration of 1×10^{-5} M and duplex DNA was added in 1×10^{-7} M aliquots from 1×10^{-7} to 2×10^{-6} M.

to account for its greater length [$K_{A\text{-}12mer} = 0.33$ ($K_{A\text{-}18mer}$) $= 1.2\times10^{5}$ M^{-1}]. Largest association constants were observed for the complex of mimetic **1b** and 18-mer d(A9T9)$_2$ (Table 1). The other compounds **2**–**4** bound more weakly, which shows once again, that the hydrophobic core and recognition strand are both needed for high affinity association.

The zinc finger motif binds the major groove of DNA through H-bond formation between the positively

Table 1. Association constants for compounds **1b–4** binding to DNA[a]

Compd	mDd $K_A \times 10^{-4}$ (M^{-1})	d(A9T9)$_2$ $K_A \times 10^{-4}$ (M^{-1})
1b	10.4 (0.4)[b]	18.9 (1.4)
1b + 0.5 M NaCl	7.5 (0.1)	2.4 (0.5)
2	2.0 (0.2)	3.3 (0.7)
3	3.0 (0.1)	3.8 (0.4)
4	2.4 (0.1)	3.5 (0.4)

[a]Determined at 25 °C, 0.1 M phosphate buffer, pH 7.0 using a modified Stern–Volmer equation.[16]
[b]Standard deviations are given in parentheses.

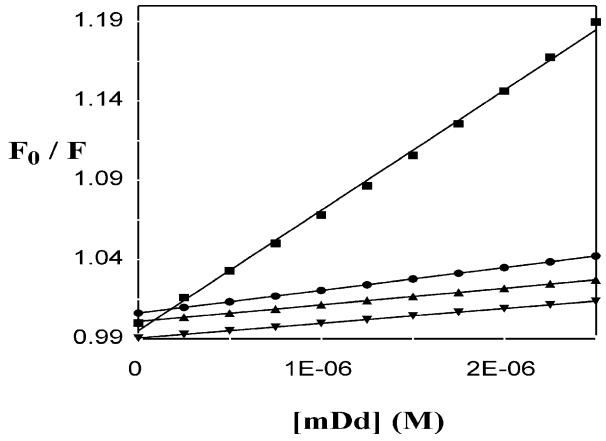

Figure 2. Representative Stern–Volmer plots that were used to derive association constants from fluorescence quenching assays. Shown are mimetic **1b** (■) and compounds **3** (●), **4** (▲), and **2** (▼) held at 1×10^{-5} M with the addition of mDd in 1×10^{-7} M aliquots from 1×10^{-7} M to 2×10^{-6} M.

charged side chains of Arg and His with guanines. Mimetic **1b**, however, binds d(A9T9)$_2$ more tightly than mDd. To help determine whether the mimetic fingers bind to a groove, the phosphate backbone, or other binding mode, association constants were obtained for the complexes in a 0.5 M NaCl/0.1 M buffer (phosphate, pH 7.0) solutions. A large drop in K_A is observed for mimetic **1b** binding to d(A9T9)$_2$ (85% reduction), whereas a much smaller reduction in K_A is observed for mDd association (25% reduction). Thus, the complex formed with d(A9T9)$_2$ has a more substantial electrostatic component than the one formed with mDd. This result suggests a different binding mode for mimetic **1b** interacting with d(A9T9)$_2$; most likely, one that involves interactions with the phosphate backbone. After correcting for the longer length duplex of d(A9T9)$_2$ by reducing its K_A by 33% (18-mer d(A9T9)$_2$ versus 12-mer mDd), mimetic **1b** has about a 5-fold preference for mDd compared to d(A9T9)$_2$ in solutions containing a high salt concentration.

CD spectroscopy. The CD profile of mDd changed significantly in the presence of mimetic **1b** (Fig. 3A). A decrease in molar ellipticity occurred for the strong positive band at 277 nm (23% reduction in intensity at λ_{277} in the presence of 3 equivalences of mimetic **1b**) with the gradual addition of mimetic **1b** (1, 2, and 3 molar equivalences). The greater amount of noise that occurs at smaller wavelengths is caused by the large concentration of DNA used in the assay.

The addition of compound **3** (Fig. 3C), which is just the recognition strand, or compound **2** and **4** (data not shown) do not alter the CD profile of mDd (3% reduction in intensity at λ_{277} in the presence of 3 equivalences of compound **3**). A slight reduction in the CD spectra (<5% of the absorbance observed for the mDd assay) occurs with the addition of a low percentage of DMSO that occurs with the addition of the template. The lack of change in the CD spectrum for compounds **2–4** with DNA suggests that their interaction with DNA does not alter the structure of the duplex. The lack of binding of the dansyl group with mDd is consistent with Schneider's work that showed that the dansyl group interacts with DNA only weakly.[19] This result is important because it suggests that the changes in the CD profile of mDd that occur with the addition of mimetic **1b** is caused by the positively charged amino acids. Nearly the same CD changes were observed for mimetic **1a** as with mimetic **1b**, which verifies that the dansyl moiety was not responsible for the changes observed in the spectra of mDd even when covalently linked to mimetic **1a**.

Smaller changes in the CD profile of d(A9T9)$_2$ were observed with the addition of mimetic **1b** and compound **3** (13% reduction in intensity at λ_{284} and λ_{248} in the presence of 3 equivalences of mimetic **1b** or compound **3**, Fig. 3B and D) than observed for mimetic **1b** binding mDd. Changes in the CD profiles of d(A9T9)$_2$ bound to mimetic **1b** and compound **3** are similar, which suggests that they use a similar mode of binding to d(A9T9)$_2$. The addition of 0.5 M NaCl to the buffered solutions of either mDd or d(A9T9)$_2$ produced only a small change (<5%) in the intensity of the observed CD spectra.

Note, under high salt conditions, the melting temperature of the duplexes were raised (for mDd, $T_{m,buffer} = 40 \pm 1$ °C, $T_{m,NaCl} = 50 \pm 1$ °C and d(A9T9)$_2$, $T_{m,buffer} = 39 \pm 1$ °C, $T_{m,NaCl} = > 47$ °C). These results show that the changes in K_A's observed with the addition of NaCl are caused by changes in the interaction energies between mimetic **1b** and the duplexes instead of changes in the properties of the duplexes.

Estimation of structure. One purpose of this research was to explore the effect that the structure of the recognition strand has on DNA recognition. Strongest binding of DNA occurs for mimetics **1a**,**b**, which contain the scaffold as well as the recognition strand (Table 1). Lowest energy structures were calculated for mimetic **1b** and compound **3** (Monte Carlo search procedure, MMFF94 force field as presented by Spartan Pro) to determine if the scaffold enhanced or diminished the structure of the recognition strand. Once the lowest energy structures are overlaid (Fig. 4), it is seen that the scaffold most likely enhances structure by greatly reducing the freedom of motion of the side chains. Thus, the side chains of mimetics **1a**,**b** should have a greater preorganization for DNA recognition.

Evidence for the preorganization was sought in the thermodynamic profiles of the DNA–template complexes.

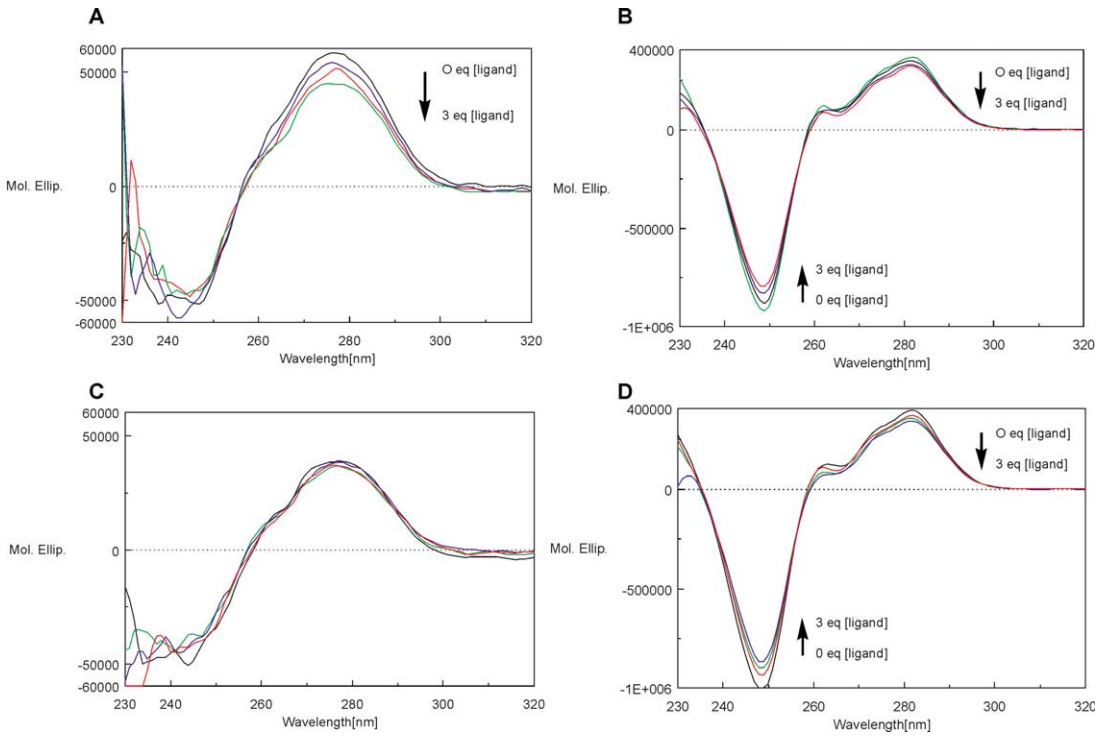

Figure. 3. Addition of 1–3 equivalences of mimetic **1b** (or **1a**) gives a decrease in the ellipticity at 277 nm of (A) mDd (5×10^{-5} M), whereas (C) compound **3** does not at 25 °C in a 0.1 M phosphate buffer at pH 7.0. A lesser reduction in ellipticity of $d(A9T9)_2$ (5×10^{-5} M) is observed with the addition of 1–3 equivalences of (B) mimetic **1b** and (D) compound **3** than observed with mDd under the same conditions.

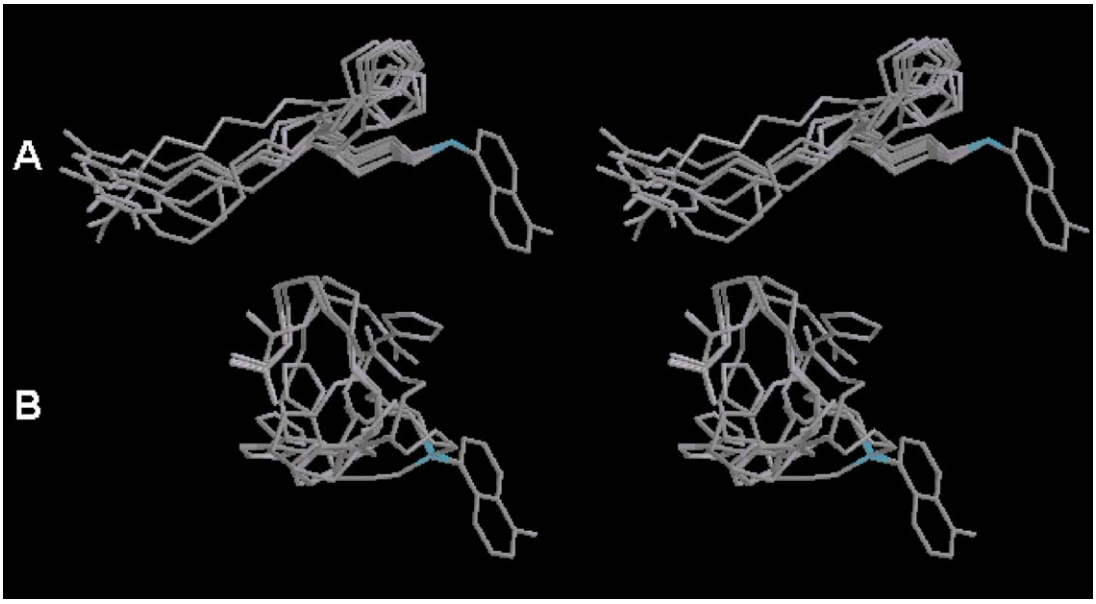

Figure 4. Stereoviews of the low energy structures of the recognition strands of (A) mimetic **1b** and (B) compound **3**, which are overlaid on the dansyl group. Only the basic carbon framework and amines of the side chains are shown for clarity. The hydrophobic scaffold of mimetic **1b**, also removed for clarity, reduces the freedom of motion of the side chains.

Heats of formation were obtained for mimetic **1b** and compound **3** by performing microcalorimetric experiments (Table 2). By combining the binding free energies—determined from the fluorescence assays—with the heats of formation, changes in the entropic energies that occur upon association were obtained. Association is enthalpically driven for all the complexes measured. As predicted, compound **3** suffers a greater loss of entropy, which is consistent with it having less structure. The modeling results also showed that the average distance between the side chains for mimetics **1a**,**b** is approximately 10 Å, which is farther apart than the side chains that form H-bonds with DNA in zinc finger 2 of Zif268. This distance more closely matches the distance between the Arg residues of zinc finger 1 or 3 (ca. 7 Å) of Zif268, which bind alternating G-residues.[13]

Discussion

Most of the experimental results are consistent with the mimetics **1a**,**b** binding in a groove of mDd and at the edge or phosphate backbone of $d(A9T9)_2$. The most compelling evidence was observed in the CD profiles (Fig. 3), where large reductions in the molar ellipticity of mDd occurred with the addition of mimetic **1a** or mimetic **1b**. Groove binding unstacks the bases, producing a reduction in the intensity of CD bands.[20] Interactions with the phosphate backbone is another possible binding mode. Polypeptides that contain multiple positively charged groups can undergo nonspecific binding to DNA and alter the shapes of CD traces, however, produce little to no change in the intensities of the bands.[21] Because this mode of binding is nonspecific and if it occurred in both complexes investigated in this study, then similar changes in the CD profiles would have been obtained for mimetics **1a**,**b** binding to mDd and to $d(A9T9)_2$. Intercalation does not seem likely since the scaffold contains a single aromatic ring with bulky substituents. Dansyl interacts very weakly with DNA,[19] and we discovered that the same reduction in ellipticity was observed for mDd with the addition of mimetic **1a**, which does not contain dansyl, as with mimetic **1b**.

The magnitude of the association constants supports the existence of different binding modes. Association constants for mimetics **1a**,**b** ($>10^5$ M^{-1}) are within the range generally observed for compounds that bind to a groove of DNA or intercalate between their bases (10^5–10^{10} M^{-1} and 10^6–10^{11}, respectively).[22,23] Compounds that bind to the edge or through partial insertion binding modes have K_A's in the range of 10^4 M^{-1}. Although mimetics **1a**,**b** bound both DNA targets with similarly large K_A's, the large difference in the salt effect suggests that mimetics **1a**,**b** bind in a groove of mDd, protected from solvent, whereas they are exposed when bound to $d(A9T9)_2$. The 85% reduction in the K_A for the complex of mimetic **1b** with $d(A9T9)_2$ caused by the addition of NaCl is consistent with a strong electrostatic component for this association. This result is consistent with binding the phosphate backbone of DNA, which has a high axial charge density.

Using methods developed by Record, analysis of the salt effect can provide an approximate number of cations released upon association ($SK = \delta \log [K_{obs}]/\delta \log [M^+]$).[24] Even though our experiments were performed under only two different salt concentrations (0.1 M phosphate and 0.5 M NaCl/0.1 M phosphate), the crude SK value for the dication mimetic **1b** binding to $d(A9T9)_2$ is consistent with the release of one or two Na^+ ions upon complexation ($SK = 1.3$). However, mimetic **1b** binding to mDd had a much smaller SK value ($SK = 0.2$), which suggests that electrostatic interactions are not an important component for its association with mDd. This lower salt effect is consistent with our hypothesis that mimetic **1b** binds in a groove of mDd without interacting significantly with the phosphate backbone.

The highly exothermic complexes formed between mimetics **1a**,**b** and the duplexes are consistent with groove binding. Generally, the driving force for compounds that bind in a groove or intercalates between the bases is a large favorable change in enthalpy.[22] Favorable enthalpic energy arises through H-bond formation between the side chains and the bases and through favorable electrostatic and van der Waals interactions. Release of water molecules from hydrophobic surfaces and cations from the phosphate backbone provides for a favorable entropic term. The large hydrophobic scaffold of mimetics **1a**,**b** contributes significantly to the binding energy; the full mimetic binds DNA stronger than its individual components. Chaires has parsed the free energy of the minor groove-binding Hoescht 33258 dye and found that the major source of free energy was the hydration term.[25] Thus, the classic hydrophobic effect, which accounts for energies involved in the dehydration of the contacting points that interact in the complex, is the driving force for association. Our study further shows that a more preformed binding site of a ligand contributes significantly to the entropic term for association. Mimetic **1b** and compound **3** have a large favorable enthalpic term for association to either duplex, but compound **3**, lacking a rigidifying scaffold, suffers a larger loss of entropic energy (Table 2). The thermodynamic profile for compound **3**, however, is not consistent with it binding through an edge or partial insertion mode. Association between DNA and non-sequence-specific, polycharged peptides generally have a favorable entropic term.[26] It may well be that a greater number of cationic side chains than the two of the mimetic fingers are needed to obtain a significant amount of favorable entropic energy from cation release.

Analysis of the data suggests that mimetics **1a**,**b** bind to a groove of mDd and to the edge or phosphate backbone of $d(A9T9)_2$. Combining the results with what is known about the properties of the major and minor grooves of DNA, we hypothesize that mimetics **1a**,**b** bind in the major groove. Minor groove binding occurs mainly at AT rich regions because the amino group of guanine blocks H-bond formation at the N3 of guanine and C2 of cytosine.[22] Binding in the major groove favors G-rich regions because of the potential additional H-bond formation. Extensive studies have shown that Arg has the strongest preference for associating with guanine in the major groove as compared to the other bases.[27] As stated previously, zinc fingers of Zif268 form H-bonds with guanine bases in the major groove. Another important factor is the size and shape differences of the major and minor grooves,

Table 2. Thermodynamic parameters for the mimetic finger **1b** and compound **3** binding to the DNA duplexes

Complex	ΔG°[a] (kcal/mol)	ΔH°[b] (kcal/mol)	$T\Delta S^{\circ}$ (kcal/mol)
1b + mDd	−6.8 (0.1)[c]	−12.8 (2.5)	−6.0 (2.5)
1b + $d(A9T9)_2$	−7.2 (0.1)	−14.6 (2.4)	−7.4 (2.4)
3 + mDd	−6.1 (0.1)	−20.0 (4.6)	−13.9 (4.1)
3 + $d(A9T9)_2$	−6.2 (0.1)	−16.4 (3.0)	−10.2 (3.0)

[a]Values obtained from Table 1.
[b]Determined at 25 °C, 0.1 M phosphate buffer, pH 7.0.
[c]Standard deviations are given in parentheses.

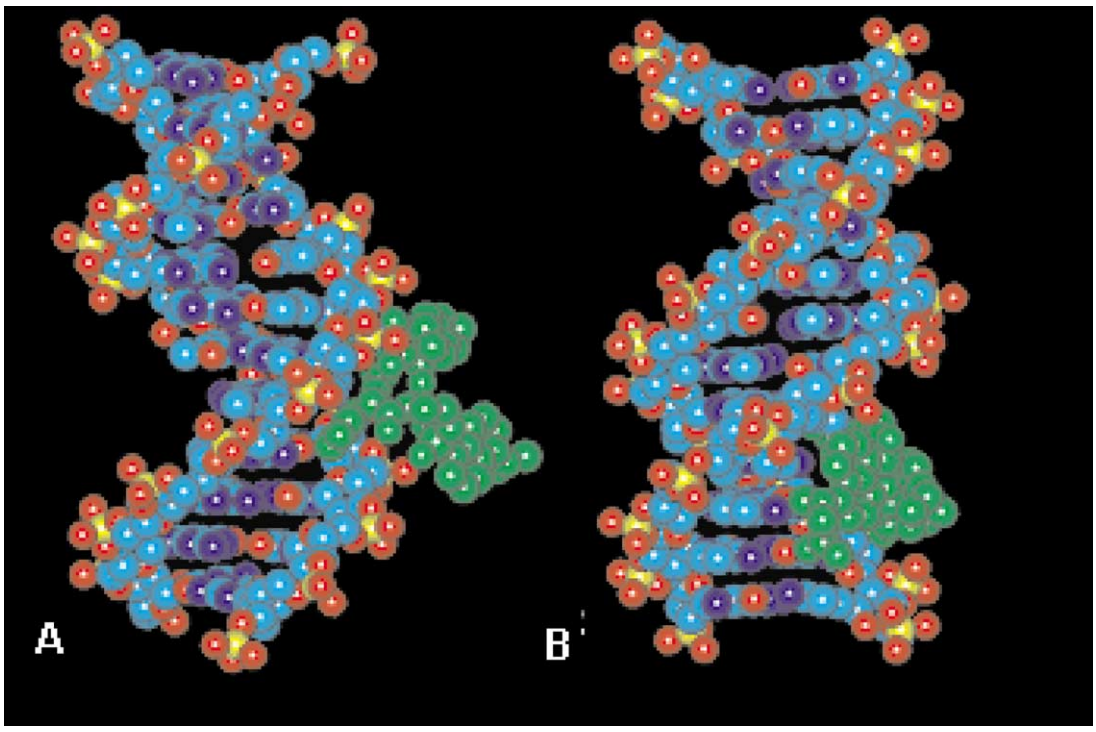

Figure 5. Energy minimized complexes (MM+ forcefield as presented by HyperChem) of mimetic **1b** (green) bound to the (A) minor and (B) major groove of mDd. Mimetic **1b** is more deeply buried in the major groove as compared to the minor groove.

and shape selectivity is an important component for DNA recognition.[28] Minor grooves are narrower than the major groove, and generally, bind small or relatively flat compounds. Molecular mechanics calculations were performed on mimetic **1b** bound to the major and minor groove of mDd to determine their likely structures. The results show that mimetic **1b** fits snuggly into the major groove, whereas only its side chains can fit into the minor groove (Fig. 5). Besides maximizing the number of favorable contacts, removing hydrophobic groups from water provides for a substantial amount of free energy for binding,[25] which appears to be only possible with incorporation of the mimetic within the major groove of mDd. Furthermore if minor groove binding does occur for both mDd and $d(A9T9)_2$, then each complex should have had more similar physical properties.

Conclusion

Examination of the X-ray structures of the Zif268 protein has led to the suggestion that its fingers use a very simple mechanism to bind G-rich regions within the major groove of DNA. Our studies show that a simple dipeptide Ac-Arg-His-NH-DAE, not surprisingly, interacts only weakly with DNA at either AT or GC sites. Placement of this recognition strand onto a hydrophobic scaffold significantly improves the dipeptide's ability to recognize DNA. The results of molecular mechanics calculations suggest that one effect of placing an aromatic ring below the recognition strand is a significant reduction in the molecular motion of the side chains. This additional structure most likely is partially responsible for the smaller loss of entropic energy observed with the association of mimetic **1b** with DNA, as compared to the dipeptide. The hydrophobic scaffold should also contribute to the favorable change in enthalpy that occurs with binding through van der Waals interactions and by partially desolvating the side chains. Although the thermodynamic profiles for mimetic **1b** binding of GC- and AT-rich DNA are similar, most experimental results suggest that mimetic **1b** binds in the major groove of GC-rich regions, whereas it binds to the edge or phosphate backbone of $d(A9T9)_2$. Selectivity for duplexes containing GC residues was observed at a high salt concentration (0.5 M NaCl). The association constants are on the order of 10^5 M^{-1}, which is far from the 10^9 M^{-1} association constant observed for Zif268 binding its DNA target,[5c] albeit Zif268 binds with three fingers held in a tandem array. We postulate that the synthetic scaffold described in this report can be further decorated to endow a series of recognition strands with greater structure to increase their affinity and specificity for a DNA target.

Experimental

Instrumental analysis

NMR spectra used for conformational analysis were measured in $CDCl_3$ using a Bruker AMX400 spectrometer operating at 400.14 MHz for proton and 100.23 MHz for carbon nuclei. Chemical shifts are reported in ppm and referenced to an internal TMS standard. All syntheses were carried out under positive argon pressure, and DMF was freshly distilled under vacuum over $MgSO_4$. Other solvents and reagents were used as purchased. A MEL-TEMP (Laboratory Devices) apparatus was used to determine the melting points

of the compounds; these values are given uncorrected. HPLC analysis was performed on a Shimadzu 10A series HPLC using a C18 reversed-phase column and water (0.1% TFA)/CH_3CN as the eluent. UV–Vis titrations were performed on a Hewlett Packard Kayak XA series spectrophotometer. Water for the HPLC assays was purified on a Millipore water purification system.

All binding titrations were conducted in a 0.1 M phosphate buffered pH 7.0 solution at 298 K unless otherwise noted. mDd and $d(A9T9)_2$ were purchased as precipitates from MWG-Biotech and dissolved in the buffered solution. Annealing was performed by heating the samples at 80 °C for 15 min, letting them cool to room temperature for 2 h, and then storing them at 4 °C. DNA concentrations were determined by measuring the absorbances at $\lambda_{max} = 259$ nm and converting these values to concentrations using calculated molar extinction coefficients.

Fluorescence quenching data were acquired on a Perkin–Elmer LS50B luminescence spectrometer and processed using FL Win v3.0 as provided by the hardware manufacturer (Perkin–Elmer Corp., CT, USA). The titrations were performed by adding ten 2.5 μL (5×10^{-7} M) injections of a DNA stock solution (0.5 mM, 0.1 M phosphate buffer) to compounds **1b–4** (2.5 mL, 1×10^{-5} M, 0.1% DMSO/0.1 M phosphate buffer, pH 7.0) in a 1-cm quartz cell at room temperature. Data was acquired at 570 nm, and was corrected for the intrinsic DNA fluorescence at this wavelength. Association constants were derived from a linear regression analysis of the best-fit modified Stern–Volmer plots.

Circular dichroism experiments were performed on a Jasco J-715 spectropolarimeter. Measurements were taken after the addition of 8-μL aliquots of stock solutions (2.5 mM, 25% DMSO/0.1 M phosphate buffer) of compounds **1–4** into a 1-mm quartz cell containing 200 μL of a 5×10^{-5} M DNA solution (0.1 M phosphate buffer). Data was acquired, and the changes in molar ellipticity were determined using J-700 Standard Analysis for Windows v1.35.01 (Easton, MD, USA).

Calorimetric titrations were carried out on a MicroCal MC-2 isothermal scanning calorimeter. Experiments were conducted by adding 4-μL injections of a stock solution (0.33 mM, 3% DMSO/0.1 M phosphate buffer, pH 7.0) of mimetic **1b** or compound **3** into a cell containing 1.37 mL of a 5×10^{-6} M DNA (0.1 M phosphate buffer, pH 7.0) solution. Data acquisition and processing were carried out using Omega v2.9 (Northampton, MA, USA). Heats of association were determined by subtracting the heats of dilution of mimetic **1b** or compound **3** into the buffered solution from the experimentally observed heats. ΔH° values are reported as averages of six injections.

DNA melting experiments were performed on a Perkin–Elmer Lambda 20 spectrometer with a jacketed eight-cell changer. Temperature was controlled by a HAAKE A81 digital circulating bath, and measurements of a sample's absorbance at 260 nm were taken at 1 °C intervals from 10 to 60 °C. Data was acquired using UV WinLab v2.80.03 as provided by Perkin–Elmer (Norwalk, CT, USA). Concentrations of the DNA were ca. 10^{-7} M, and the T_m values reported are an average of two runs.

Molecular modelling

Low energy structures of mimetic **1b** and compound **3** were determined through a Monte Carlo search method using the MMFF94 force field (package procedure of Spartan Pro, Wavefunction, Inc. Irvine, CA, USA). Generally, over 1500 structures were created and analyzed for potential energy through a simulated annealing process starting at 5000 K and ending at 300 K. The chosen set of lowest energy conformers were within 1 kcal/mol of the global minimum structure. To make a meaningful comparison, the structures were overlaid on the dansyl ring.

Docking interactions between mimetic **1b** and mDd were determined by first obtaining the energy minimized structure of mDd using a conjugate gradient method (Polak-Ribiere) to a rms gradient of 0.01 kcal/(mol·Å) (molecular mechanics calculations, MM+ force field as presented by HyperChem, Hypercube, Inc. Gainesville, FL, USA). Energy minimized mimetic **1b**, obtained from the Monte Carlo simulations, was placed at various positions along the major and minor grooves of mDd. Energy minimized complexes were obtained by holding the mDd's trajectories constant and reminimizing mimetic **1b** using a conjugate gradient method (Polak-Ribiere) to a rms gradient of 0.01 kcal/(mol·Å) (molecular mechanics calculations, MM^+ force field). The lowest energy complexes had mimetic **1b** bound within the major groove of mDd through interactions with alternating guanines.

***N*-Arg(MTS)-2,3-dicarboxyimido-5,6-benzobicyclo[2.2.1]-heptane (6).** To a solution of anhydride **5**[15] (537 mg, 2.50 mmol) in DMF (5 mL) was added Arg(MTS) (937 mg, 2.63 mmol) and DIEA (0.458 mL, 2.63 mmol). After stirring for 3 h at room temperature, TLC analysis showed no starting anhydride, and CDI (853 mg, 5.26 mmol) was added. The solution was stirred overnight. The reaction mixture was concentrated in vacuo, dissolved in EtOAc (100 mL), extracted with 5% HCl (3×10 mL) and then brine (20 mL). The organic phase was concentrated to give 1.14 g (83%) of compound **6** as a white solid (mp 228–228.4 °C) that was used without further purification. ^{1}H NMR: (400 MHz, 10% DMSO-d_6/$CDCl_3$) δ 7.14 (m, 2H), 7.03 (m, 2H), 6.90 (s, 2H), 6.42 (s, 2H), 6.05 (bs, 1H), 4.00 (bt, 1H), 3.79 (m, 2H), 3.61 (m, 1H), 3.51 (m, 1H), 2.91 (m, 2H), 2.82 (m, 2H), 2.70 (s, 6H), 2.27 (s, 3H), 2.08 (d, $J = 9.1$ Hz, 1H), 1.97 (d, $J = 9.1$ Hz, 1H), 1.66 (m, 1H), 0.83 (m, 2H), 0.41 (m, 2H). ^{13}C NMR: (100 MHz, 10% DMSO-d_6/$CDCl_3$) δ 175.8, 175.7, 170.0, 156.3, 142.5, 139.9, 138.5, 137.5, 131.1, 126.9, 126.8, 122.5, 53.0, 51.5, 47.6, 46.8, 45.9, 45.7, 25.4, 25.3, 22.6, 20.5. HRMS m/z calculated for $C_{28}H_{32}N_4O_6S$ (MNa^+) 575.1985, found 575.1940.

***N*-(Arg-His methyl amide)-2,3-dicarboxyimido-5,6-benzobicyclo[2.2.1]-heptane di- fluoroacetate (1a).** A solution

of compound **6** (206 mg, 0.373 mmol), histidine methyl ester dihydrochloride (85 mg, 0.35 mmol), DIEA (0.124 mL, 0.708 mmol), DCC (73 mg, 0.35 mmol), and HOBT hydrate (48 mg, 0.35 mmol) in THF was allowed to stir for 1 h at 0 °C and an additional 10 h at room temperature. After DCU was filtered off, the crude reaction mixture was concentrated in vacuo, taken up in 50 mL ethyl acetate, extracted with 1 M KOH (3×5 mL), dried ($MgSO_4$) and concentrated to yield 220 mg (88%) of a white solid, which was used without further purification. The crude product (0.313 mmol) was dissolved in DMF (1 mL) and treated with 40% methyl amine in H_2O (0.270 mL, 3.13 mmol) at room temperature for 24 h, at which point TLC analysis showed no remaining starting material. The crude methyl amide was concentrated in vacuo and a solution of TFA/TFMSA/thioanisole (8:1:1, 5 mL) was added. The reaction mixture was allowed to stir for 48 h, at which time residual solvents were removed in vacuo, and the remaining residue was subjected to HPLC purification to yield 50 mg (18% from **6**) of mimetic **1a** as an amber oil. ^{1}H NMR: (400 MHz, CD_3OD) δ 8.79 (s, 1H), 7.32 (d, J = 7.6 Hz, 1H), 7.29 (s, 1H), 7.23–7.12 (m, 3H), 4.64 (dd, J = 8.4 Hz, J = 8.0 Hz, 1H), 4.14 (t, J = 8 Hz, 1H), 3.82–3.66 (m, 4H), 3.18 (m, 1H), 3.06–2.87 (m, 6H), 2.03 (bt, 2H), 1.67 (m, 1H), 0.96 (m, 1H), 0.70–0.50 (m, 2H). HRMS m/z calculated for $C_{26}H_{32}N_8O_4$ (MH^+) 521.2625 found 521.2606.

His-DAE (8). Boc-His(Boc) **7** (217 mg, 0.849 mmol), DANSA (250 mg, 0.849 mmol) and HOBT hydrate (115 mg, 0.849 mmol) were combined in 3 mL THF / 0.5 mL DMF and cooled to 0 °C. After stirring at 0 °C for 1 h, DCC (175 mg, 0.849 mmol) was added, and the solution was allowed to react for an additional 10 h. DCU was filtered off, and the filtrate was concentrated to dryness. The resulting residue was taken up in 50 mL ethyl acetate and extracted with 1 M KOH (3×2 mL). The aqueous layer was extracted with ethyl acetate (10 mL), and the combined organic phases were dried ($MgSO_4$), and concentrated to give 550 mg (95%) of a yellow solid. This crude solid was dissolved in TFA (4 mL) and DMS (1.5 mL), and allowed to stir at room temperature for 1.5 h. The reaction mixture was concentrated in vacuo, diluted with methanol (3 mL) and concentrated in vacuo. This process was repeated three times to remove residual TFA. Ethyl acetate (50 mL) was added, and the solution was extracted with 5% HCl (3×10 mL). The aqueous extract was made basic (pH = 14) by the addition of solid KOH, and the resulting aqueous solution was extracted with ethyl acetate (5×10 mL). The organic extracts were combined, dried ($MgSO_4$) and concentrated in vacuo to give 220 mg (65% from **7**) of a yellow solid (mp 71–73 °C), which was used without further purification. ^{1}H NMR: (400 MHz, CD_3OD) δ 8.86 (s, 1H), 8.55 (t, J = 8.6 Hz, 2H), 8.23 (d, J = 6.8 Hz, 1H), 7.68 (t, J = 7.3 Hz, 1H), 7.57 (d, J = 8.5 Hz, 1H), 4.21 (t, J = 6.9 Hz, 1H), 3.38–3.24 (m, 4H), 3.09 (s, 3H), 2.96 (m, 2H). ^{13}C NMR: (100 MHz, CD_3OD) δ 173.8, 173.6, 169.3, 168.0, 133.9, 130.5, 57.2, 52.0, 47.3, 46.7, 35.9, 34.4, 33.6, 33.1, 26.0, 25.2, 24.6, 14.8. HRMS m/z calculated for $C_{20}H_{26}N_6O_3S$ (MNa^+) 453.1677, found 453.1685.

***N*-(Arg-His-DAE)-2,3-dicarboxyimido-5,6-benzobicyclo[2.2.1]heptane trifluoroacetate (1b).** His-DAE, **8**, (44 mg, 0.054 mmol), HOBT hydrate (7.0 mg, 0.049 mmol) and DCC (10 mg, 0.049 mmol) was added to a solution of compound **6** (28 mg, 0.049 mmol) in DMF (3 mL) at 0 °C. The mixture was stirred for 1 h at 0 °C before warming to room temperature. After 24 h, DCU was filtered off, and the filtrate was concentrated in vacuo to remove DMF. The residue was taken up in 50 mL ethyl acetate and extracted with 1 M KOH (3×2 mL). Once the organic layer was dried ($MgSO_4$) and concentrated in vacuo a yellow solid was obtained. The crude product was then dissolved in TFA/TFMSA/thioanisole (8:1:1, 4 mL) and was allowed to stir at room temperature for 24 h. After removal of residual solvents in vacuo, the crude residue was diluted with 5 mL diethyl ether to precipitate a white granular solid that was subjected to HPLC purification. The trifluoroacetate salt of mimetic **1b** was obtained as a yellow solid (55 mg, 39% from **6**, mp 133.5–135.0 °C). ^{1}H NMR: (400 MHz, CD_3OD) δ 8.76 (s, 1H), 8.58 (d, J = 8.5 Hz, 1H), 8.38 (d, J = 8.5 Hz, 1H), 8.19 (d, J = 7.0 Hz, 1H), 7.64 (m, 2H), 7.37 (d, J = 7.5 Hz, 1H), 7.27 (s, 1H), 7.20–7.11 (m, 4H), 4.62 (bt, 1H), 4.12 (t, J = 6.9 Hz, 1H), 3.77–3.68 (m, 4H), 3.32–3.28 (m, 3H), 3.10 (m, 1H), 2.94 (s, 6H), 2.87 (m, 2H), 2.02 (m, 2H), 1.64 (m, 1H), 1.84 (m, 1H), 0.95 (m, 1H), 0.59 (m, 1H). ^{13}C NMR (100 MHz, CD_3OD): δ 172.2, 169.2, 168.1, 143.2, 142.7, 140.8, 140.1, 126.6, 126.1, 125.7, 125.0, 123.5, 52.3, 52.1, 47.1, 46.4, 36.8, 36.2, 34.3, 25.9, 14.6. HRMS m/z calculated for $C_{39}H_{47}N_{10}O_6S$ (M +) 783.3495, found 783.3468.

***N*-[Gly-Gly(OCH$_3$)]-2,3-dicarboxyimido-5,6-benzobicyclo[2.2.1]heptane (9).** A solution of glycinyl–glycine methyl ester hydrochloride (526 mg, 2.88 mmol), anhydride **5** (555 mg, 2.59 mmol) and DIEA (1.00 mL, 5.76 mmol) in DMF (2 mL) was allowed to stir at room temperature for 2 h, at which time TLC analysis showed no remaining anhydride. CDI (546 mg, 3.37 mmol) was added, and the reaction mixture was stirred overnight. The solution was concentrated, taken up in ethyl acetate (200 mL) and then extracted with 5% HCl (3×10 mL) followed by brine (20 mL). Concentration of the organic layer gave 680 mg (91%) of compound **9** as a white solid (mp 160.5–161.2 °C), which was used without further purification. ^{1}H NMR: (400 MHz, DMSO-d_6) δ 8.23 (t, J = 5.4 Hz, 1H), 7.08 (s, 4H), 3.76 (s, 1H), 3.74 (s, 1H), 3.70 (s, 2H), 3.66 (s, 2H), 3.57 (s, 3H), 3.15 (s, 2H), 1.91 (s, 2H). ^{13}C NMR: (100 MHz, MeOH-d_4) δ 178.5, 171.4, 169.1, 144.1, 128.1, 123.9, 53.0, 52.7, 49.3, 47.7, 42.0, 40.8. HRMS m/z calculated for $C_{18}H_{18}N_2O_5$ (MH^+) 343.1294, found 343.1284.

***N*-[Gly-Gly]-2,3-dicarboxyimido-5,6-benzobicyclo[2.2.1]-heptane (10).** LiOH (0.261 mL, 0.241 mmol) was added to a solution of methyl ester **9** (75 mg, 0.22 mmol) in THF (1.5 mL). The reaction mixture was stirred for 2 h at room temperature and concentrated to dryness. Ethyl acetate (50 mL) was used to dissolve the crude material, which was extracted with 5% HCl (3×1 mL) and brine (5 mL). Organic phases were combined, dried ($MgSO_4$) and concentrated to give 45 mg (63%) of compound **10** as a white solid (mp 189–190 °C), which was used without

further purification. ^{1}H NMR: (400 MHz, DMSO-d_6) δ 8.11 (t, J = 5.6 Hz, 1H), 7.08 (s, 4H), 3.73 (s, 2H), 3.66 (s, 2H), 3.65 (s, 2H), 3.15 (s, 2H), 1.93 (s, 2H). ^{13}C NMR (100 MHz, CD_4OD): δ 178.6, 172.5, 170.0, 144.1, 128.2, 128.1, 128.0, 124.0, 123.9, 53.0, 52.7, 47.8, 47.7, 42.0, 41.9, 40.8, 24.4. HRMS m/z calculated for $C_{17}H_{16}N_2O_5$ (MH+) 329.1137, found 329.1142.

***N*-(Gly-Gly-DAE)-2,3-dicarboxyimido-5,6-benzobicyclo[2.2.1]heptane trifluoroacetate (2).** DANSA (50 mg, 0.17 mmol) and HOBT hydrate (23 mg, 0.17 mmol) was added to a solution of acid **10** (51 mg, 0.15 mmol) in DMF (3 mL) at 0 °C. After stirring the solution at 0 °C for 1 h, DCC (35 mg, 0.17 mmol) was added and the reaction mixture was left to stir overnight at room temperature. The precipitated DCU was filtered off, and the filtrate was concentrated in vacuo to remove DMF. The resulting residue was taken up in 50 mL ethyl acetate and extracted with 1 M KOH (3×2 mL). The organic layer was dried ($MgSO_4$) and concentrated to give a yellow solid that was subjected to HPLC purification. Compound **2** was obtained as a yellow solid (30 mg, 27%), mp 141.4–142.2 °C. ^{1}H NMR: (400 MHz, $CDCl_3$) δ 8.54 (d, J = 1.8 Hz, 1H), 8.32 (d, J = 1.8 Hz, 1H), 8.21 (d, J = 1.8 Hz, 1H), 7.53 (dd, J = 1.8 Hz, J = 1.8 Hz, 2H), 7.22 (m, 2H), 7.20 (d, J = 1.8 Hz, 1H), 7.12 (d, J = 1.8 Hz, 2H), 6.05 (t, J = 1.8 Hz, 1H), 6.42 (t, J = 1.8 Hz, 1H), 6.77 (t, J = 1.8 Hz, 1H), 3.86 (s, 2H), 3.67 (s, 2H), 3.66 (s, 2H), 3.50 (s, 2H), 3.27 (m, 2H), 3.01 (m, 2H), 2.88 (s, 6H), 2.11 (d, J = 1.8 Hz, 1H), 1.94 (d, J = 1.8 Hz, 1H). ^{13}C NMR (100 MHz, $CDCl_3$): δ 177.4, 169.7, 166.7, 152.2, 142.7, 134.9, 130.7, 130.2, 129.8, 129.6, 128.6, 127.4, 127.3, 123.4, 123.1, 119.1, 115.5, 52.5, 48.2, 48.0, 46.5, 45.6, 43.3, 42.8, 41.3, 39.9. HRMS m/z calculated for $C_{31}H_{33}N_5O_6S$ (MH+) 604.2230, found 604.2260.

Boc-Arg(Boc)$_2$-His-DAE (12). Boc-Arg(Boc)$_2$ **11** (57 mg, 0.12 mmol), DCC (25 mg, 0.12 mmol), and HOBT hydrate (16 mg, 0.12 mmol) were dissolved in 4 mL DMF and allowed to stir at 0 °C for 1 h. His-DAE, **8**, (47 mg, 0.11 mmol) was added to the reaction mixture, and it was left to stir overnight at room temperature. Precipitated DCU was filtered off, and the residual DMF was removed in vacuo. The crude residue was taken up in 50 mL ethyl acetate, extracted with 1.0 M KOH (3×5 mL), dried ($MgSO_4$) and concentrated to yield 94 mg (99%) of compound **12** as a yellow solid (mp 122–124 °C), which was used without further purification. ^{1}H NMR: (400 MHz, $CDCl_3$): δ 9.31 (bs, 2H), 8.50 (d, J = 8.5 Hz, 1H), 8.33 (d, J = 8.6 Hz, 1H), 8.18 (d, J = 7.2 Hz, 1H), 7.79 (s, 1H), 7.68 (bs, 1H), 7.51 (m, 2H), 7.15 (m, 3H), 6.90 (s, 1H), 5.71 (bs, 1H), 4.59 (bq, 1H), 4.11 (bq, 1H), 3.98 (m, 1H), 3.87 (m, 1H), 3.21 - 2.99 (m, 4H), 2.87 (m, 6H), 1.70–1.50 (m, 6H), 1.50 (s, 9H), 1.47 (s, 9H), 1.41 (s, 9H). ^{13}C NMR (100 MHz, $CDCl_3$): δ 172.2, 171.9, 163.7, 160.8, 156.5, 155.0, 152.0, 135.5, 135.1, 130.4, 130.1, 129.8, 129.3, 128.4, 123.4, 119.4, 115.4, 84.4, 84.1, 80.7, 79.6, 60.6, 55.8, 53.4, 45.6, 44.3, 43.0, 39.8, 29.5, 29.2, 28.6, 28.5, 28.5, 28.2, 25.3, 14.4. HRMS m/z calculated for $C_{41}H_{62}N_{10}O_{10}S$ (MH+) 887.4449, found 887.4488.

Ac-Arg-His-DAE trifluoroacetate (3). Boc-Arg(Boc)$_2$-His-DAE, **12**, (94 mg, 0.11 mmol) was treated with 30% TFA in methylene chloride for 1 h at room temperature. The reaction mixture was concentrated in vacuo, diluted with 3 mL methanol and concentrated. This procedure was repeated (3×) to remove residual TFA. Ethyl acetate (50 mL) was then added, and the solution was extracted with 5% HCl (3×10 mL). The aqueous extract was made basic (pH = 14) by the addition of solid KOH, and the resulting solution was extracted with ethyl acetate (5×10 mL). The organic extracts were combined, dried ($MgSO_4$), and concentrated in vacuo. The crude tetra-trifluoroacetate (13 mg, 0.020 mmol) was dissolved in 2 mL THF and treated with LiOH (0.65 mL, 0.060 mmol) followed by acetic anhydride (2 μL, 0.020 mmol). After stirring at room temperature for 10 h, the crude solution was concentrated in vacuo to give a yellow solid that was subjected to HPLC purification. Compound **3** was obtained in a 27% yield as a yellow solid (mp 140–142.5 °C). ^{1}H NMR: (400 MHz, CD_3OD) δ 8.79 (s, 1H), 8.56 (d, J = 8.5 Hz, 1H), 8.40 (d, J = 8.6 Hz, 1H), 8.20 (d, J = 6.4 Hz, 1H), 7.63 (m, 2H), 7.40 (d, J = 7.5 Hz, 1H), 7.36 (s, 1H), 4.66 (m, 1H), 4.23 (m, 1H), 3.31–3.17 (m, 6H), 2.97–2.92 (m, 8H), 2.00 (s, 3H), 1.80 (m, 1H), 1.66 (m, 4H), 1.15 (m, 1H). ^{13}C NMR (100 MHz, CD_3OD): δ 174.4, 174.0, 172.2, 162.5, 162.2, 152.1, 137.1, 135.1, 131.2, 131.1, 130.3, 129.4, 124.9, 121.4, 118.7, 117.1, 55.1, 53.7, 46.1, 43.2, 42.1, 40.8, 29.8, 28.0, 26.5, 22.6. HRMS m/z calculated for $C_{28}H_{40}N_{10}O_5S$ (MH+) 629.2977, found 629.2924.

Acknowledgements

The authors thank the University of Cincinnati for their funding of this project. We also thank Drs. A. Stalcup for the use of the CD spectrometer, H. B. Halsall for the use of the titration flow calorimeter, and P. Tsang for insightful discussions. J.A.T. was supported by the Lange Fellowship.

References and Notes

1. (a) Jacobs, G. H. *Embo J.* **1992**, *11*, 4507. (b) Pellegrino, G. R.; Berg, J. M. *Proc. Natl. Acad. Sci. U.S.A.* **1991**, *88*, 671.
2. (a) Choo, Y.; Klug, A. *Proc. Natl. Acad. Sci., U.S.A.* **1994**, *91*, 11168. (b) Desjarlais, J. R.; Berg, J. M. *Proc. Natl. Acad. Sci. U.S.A.* **1993**, *90*, 2256.
3. (a) Segal, D. J.; Dreier, B.; Beerli, R. R.; Barbas III, C. F. *Proc. Natl. Acad. Sci. U.S.A.* **1999**, *96*, 2758. (b) Beerli, R. R.; Segal, D. J.; Dreier, B.; Barbas III, C. F. *Proc. Natl. Acad. Sci. U.S.A.* **1998**, *95*, 14628.
4. (a) Imanishi, M.; Hori, Y.; Nagaoka, M.; Sugiura, Y. *Biochemistry* **2000**, *39*, 4383. (b) Kang, J. S.; Kim, J. S. *J. Biol. Chem.* **2000**, *275*, 8742. (c) Beerli, R. R.; Dreier, B.; Barbas III, C. F. *Proc. Natl. Acad. Sci. U.S.A.* **2000**, *97*, 1495. (d) Greisman, H. A.; Pabo, C. O. *Science* **1997**, *275*, 657.
5. (a) Wang, B. S.; Pabo, C. O. *Proc. Natl. Acad. Sci. U.S.A.* **1999**, *96*, 9568. (b) Wolfe, S. A.; Greisman, H. A.; Ramm, E. I.; Pabo, C. O. *J. Mol. Biol.* **1999**, *285*, 1917. (c) Erickson-Elrod, M.; Pabo, C. O. *J. Biol. Chem.* **1999**, *274*, 19281. (d) Pomerantz, J. L.; Wolfe, S. A.; Pabo, C. O. *Biochemistry* **1998**, *37*, 965.
6. Greisman, H. A.; Pabo, C. O. *Science* **1997**, *275*, 657.

7. (a) Erkkila, K. E.; Odom, D. T.; Barton, J. K. *Chem. Rev.* **1999**, *99*, 2777. (b) Odom, D. T.; Parker, C. S.; Barton, J. K. *Biochemistry* **1999**, *38*, 5155.
8. Mizumoto, K.; Sato, N.; Kusumoto, M.; Niiyama, H.; Maehara, N.; Nishio, S.; Li, Z.; Ogawa, T.; Tanaka, M. *Cancer Lett.* **2000**, *149*, 85.
9. (a) Rodger, A.; Patel, K. K.; Sanders, K. J.; Datt, M.; Sacht, C.; Hannon, M. J. *J. Chem. Soc., Dalton Trans.* **2002**, *19*, 3656. (b) Ismail, M. A.; Sanders, K. J.; Fennell, G. C.; Latham, H. C.; Wormell, P.; Rodger, A. *Biopolymers* **1998**, *46*, 127.
10. Deubel, D. V. *J. Am. Chem. Soc.* **2002**, *124*, 5834.
11. Jamieson, E. R.; Lippard, S. *J. Chem. Rev.* **1999**, *99*, 2467.
12. Kikuta, E.; Koike, T.; Kimura, E. *J. Inorg. Biochem.* **2000**, *79*, 253.
13. Pavletich, N. P.; Pabo, C. O. *Science* **1991**, *252*, 809.
14. (a) Dickerson, R. E.; Drew, H. R.; Conner, B. N.; Wing, R. M.; Fratini, A. V.; Kopka, M. L. *Science* **1982**, *216*, 475. (b) Hare, D. R.; Wemmer, D. E.; Chou, S.-H.; Drobny, G. *J. Mol. Biol.* **1983**, *171*, 319.
15. Huebner, C. F.; Strachan, P. L.; Donoghue, E. M.; Cahoon, N.; Dorfman, L.; Margerison, R.; Wenkert, E. *J. Org. Chem.* **1967**, *32*, 1126.
16. Ren, B.; Gao, F.; Tong, Z.; Yan, Y. *Chem. Phys. Lett.* **1999**, *307*, 55.
17. Olsen, R. K.; Ramasamy, K. *J. Org. Chem.* **1985**, *50*, 2264.
18. (a) Boger, D. L.; Winston, C. T. *Bioorg. Med. Chem.* **2001**, 2511. (b) Naumann, W. *J. Chem. Phys.* **2000**, *112*, 7152. (c) Green, N. J. B.; Pimblott, S. M.; Tachiya, M. *J. Phys. Chem.* **1993**, *97*, 196.
19. Wang, X. M.; Schneider, H. J. *J. Chem. Soc., Perkin Trans. 2* **1998**, *6*, 1323.
20. (a) Gray, D. M. In *Circular Dichroism and the Conformational Analysis of Biomolecules*, Fasman, G. D., Ed., Plenum; New York, 1996; Chapter 13. (b) Chan, S. S.; Breslauer, K. J.; Hogan, M. E.; Kessler, D. J.; Austin, R. H.; Ojemann, J.; Passner, J. M.; Wiles, N. C. *Biochemistry* **1990**, *29*, 6161.
21. (a) Padmanabhan, S.; Zhang, W. T.; Capp, M. W.; Anderson, C. F.; Record, M. T. *Biochemistry* **1997**, *36*, 5193. (b) Panoupomonis, E.; Sakarellos, C.; Sakarellosdaitsiotis, M. *Eur. J. Biochem.* **1986**, *161*, 185.
22. Haq, I.; Ladbury, J. *J. Mol. Recogn.* **2000**, *13*, 188.
23. For examples of large association constants for groove binders see: (a) Pilch, D. S.; Poklar, N.; Gelfand, C. A.; Law, S. M.; Breslauer, K. J.; Baird, E. E.; Dervan, P. B. *Proc. Natl. Acad. Sci. U.S.A.* **1996**, *93*, 8306. For examples of large association constants for intercalation see: (b) Leng, F. F.; Priebe, W.; Chaires, J. B. *Biochemistry* **1998**, *37*, 1743.
24. Record, M. T.; Anderson, C. F.; Lohman, T. M. *Q. Rev. Biophys.* **1978**, *11*, 103.
25. (a) Haq, I.; Jenkins, T. C.; Chowdhry, B. Z.; Ren, J.; Chaires, J. B. *Methods Enzym.* **2000**, *323*, 373. (b) Haq, I.; Ladbury, J. E.; Chowdhry, B. Z.; Jenkins, T. C.; Chaires, J. B. *J. Mol. Biol.* **1997**, *271*, 244.
26. Mascotti, D. P.; Lohman, T. M. *Biochemistry* **1997**, *36*, 7272 and references therein.
27. (a) Han, X. G.; Gao, X. L. *Curr. Med. Chem.* **2001**, *8*, 551. (b) Gresh, N.; Perree-Fauvet, M. *J. Comp. Aid. Mol. Des.* **1999**, *13*, 123. (c) Mohammadi, S.; Perree-Fauvet, M.; Gresh, N.; Hillairet, K.; Taillandier, E. *Biochemistry* **1998**, *37*, 6165 and references therein..
28. Bostock-Smith, C. E.; Laughton, C. A.; Searle, M. S. *Biochem. J.* **1999**, *342*, 125.